*aerospace*

*Article*

# A New Flow Control and Efficiency Enhancement Method for Horizontal Axis Wind Turbines Based on Segmented Prepositive Elliptical Wings

**Xuan Bai, Hao Zhan and Baigang Mi ***

School of Aeronautics, Northwestern Polytechnical University, Xi'an 710072, China;
baixuan@mail.nwpu.edu.cn (X.B.); zhanhao@nwpu.edu.cn (H.Z.)
* Correspondence: mibaigang@163.com

**Abstract:** Flow separation occurs when wind turbines operate under large inflow conditions, which seriously affects the utilization of wind energy and reduces the output power of the blade. Therefore, a composite flow control configuration for horizontal axis wind turbines, founded on segmented prepositive elliptical wings, is proposed for efficiency enhancement. Taking a typical NREL Phase VI wind turbine as the prototype, its separation effect is evaluated by the CFD method. Then, starting from the improvement of the two-dimensional airfoil flow, the prepositive elliptic wing is designed according to the airfoil flow, and the optimal two-dimensional flow control configuration of the blade airfoil is obtained by simulation analysis. Finally, the two-dimensional configuration is extended to three-dimensional, and the aerodynamic characteristics of the blade before and after flow control are simulated and compared. The results show that, at wind speeds of 10~20 m/s, flow separation on the blade is effectively inhibited; meanwhile, the pressure difference between the pressure surface and the suction surface increases. These characteristics greatly improve the performance of wind turbine and increase its torque by more than 30%. Moreover, when the flow control effect cannot be reached, the blade torque is only reduced by approximately 2%.

**Keywords:** horizontal axis wind turbine; prepositive elliptic wing; computational fluid dynamics (CFD); flow control



**Citation:** Bai, X.; Zhan, H.; Mi, B. A New Flow Control and Efficiency Enhancement Method for Horizontal Axis Wind Turbines Based on Segmented Prepositive Elliptical Wings. *Aerospace* **2023**, *10*, 796. https://doi.org/10.3390/aerospace10090796

Received: 8 August 2023
Revised: 5 September 2023
Accepted: 6 September 2023
Published: 12 September 2023



## 1. Introduction

As an important guarantee for national development, energy supply is a solid foundation for promoting social prosperity and improving the quality of the living environment for residents. With the increasing consumption of global fossil fuels and environmental problems, new energy sources, for instance, wind energy, solar energy, and nuclear energy, have become an important research field of worldwide concern. As one of the new energy sources for sustainable development, wind energy has many advantages, such as abundant storage, wide distribution, no pollution, and so on, and has great potential. Wind turbines play a key role in wind power generation, so the evaluation of the aerodynamic performance of wind turbine blades is a crucial part in the design of wind turbines. When a wind turbine blade is in some operating states with large angles of attack, the surface is prone to flow separation, resulting in reduced aerodynamic performance of the blades. Inhibiting the flow separation on the blade surface has great significance on the improvement of the efficiency of wind turbines, and it has become one of the research hotspots in current wind energy utilization.

At present, there are mainly active and passive flow control methods applied to the wind turbine blades. Active flow control technology suppresses flow separation by introducing external energy to enhance the internal energy of the separated flow. Typical methods include blow suction control, co-flow jets, plasma ion jets, etc. These active flow control methods based on jets have been widely studied and have achieved good results in controlling the flow of wind turbine airfoils and blades [1–6]. However, because additional energy must be introduced and components such as a gas path, actuator, controller, and the power supply must be added, the design difficulty is greatly increased, and the applicability is reduced in engineering applications. In contrast, it is easier to realize the passive methods to change the characteristics of the main flow by adding auxiliary components on the external surface and mixing the airflow of the components with the main flow. For example, tip winglets [7–10], bionic leading edges [11–13], Gurney flaps [14–16], vortex generators [17–24], and other components have been added to the blades to improve the wind turbine's aerodynamic performance. Nobari et al. [7] studied a wind turbine equipped with flat winglets by the finite volume method, and the wind turbine power increased by 16% after optimization. Khaled [8] and Mourad [10] et al. researched the influence of winglet length, tilt angle, and winglet height on the aerodynamic characteristics of horizontal axis wind turbines; they pointed out that winglet configuration and setting position were important factors affecting blade performance. Abate et al. [12,13] designed and calculated the flow field characteristics of a uniformly distributed wave front wind turbine blade and found that the best effect could be achieved when the wave front was placed at 95% of the span direction, and the export power of the new configuration was increased by up to 10%. Yang et al. [15] tested the impact of changing the height and thickness of Gurney flaps on wind airfoils through wind tunnel experiments; their research showed that the height parameter of the Gurney flaps had the main influence. Wang et al. [17] adopted a vortex generator to control the separation flow of an S809 airfoil. After adding a vortex generator, the stall attack angle of the S809 was delayed from 14° to 18°, but the effect of applying it to a three-dimensional rotating blade still needs further research. Troldborg et al. [18] compared airfoils and blades with vortex generators through a numerical simulation, and the results showed that there was a complicated interaction between rotation effects and vortex generators. Suarez et al. [19] also studied the flow field characteristics after setting the vortex generators at the tip of an NREL Phase VI blade and found that the aerodynamic characteristics of the rotating blade were only slightly improved after adding the vortex generators. Mueller [20] and Baldacchino et al. [21] proposed that setting the vortex generator on the wind turbine blade makes it very sensitive to the height and chord position. Improper setting of the height will drown the vortex generator in the separation bubble, leading to the sudden stall of the blade in the early stage. Lee et al. [22] studied the effect of a vortex generator on the aerodynamic load, elastic deformation, and flow separation of a horizontal axis wind turbine blade using the fluid-structure coupling method. The results indicated that, under the condition of steady flow, the flow separation area of blade suction surface with a vortex generator was reduced, but the power was only increased by 1.04% at most. Dadamoussa et al. [23] designed vortex generators with different heights and positions to study the influence on the flow control of horizontal axis wind turbines. Their results showed that the correct selection of the vortex generator's size and position played a crucial role in improving the aerodynamic performance of wind turbine blade. Zhu et al. [24] set up a vortex generator on the two-dimensional airfoil and performed a numerical simulation. The results indicated that the separation flow was effectively suppressed and that its lift coefficient was greatly improved. However, when it was set on the three-dimensional blade, the vortex generator was completely submerged in the separation bubbles, which aggravated flow separation and reduced aerodynamic force on the blade surface. Therefore, a vortex generator design that is based on a two-dimensional airfoil is difficult to directly apply to a three-dimensional blade. In summary, active flow control technology is time-consuming and labor-intensive, and its practicability is poor, while the passive flow control method usually has problems such as low efficiency, difficult design, and additional resistance.

In consideration of above problems, this paper innovatively proposes a segmented prepositive wing–main blade composite configuration. This flow control method is passive and has the advantages of simple design, no additional input energy, easy processing, and high fault tolerance. Taking the typical NREL Phase VI wind turbine blade as the prototype, its S809 airfoil is first designed with the prepositive wing configuration. The impact of position and size of the prepositive wing on the aerodynamic performance of the airfoil is researched to find the optimal setting scheme, and its flow control mechanism is analyzed. Then, this airfoil design is applied to the blade to verify the feasibility of transferring the flow control effect from a two-dimensional design to a three-dimensional design. In addition, because the conventional vortex generator positioning near the root of the blade may cause it to stall early, five kinds of segmented prepositive wing–main blade composite configurations are designed to study the influence of the height of the elliptical wing. Through numerical simulation, the flow field characteristics of the original blade and the composite configurations are compared, and the flow control mechanism of the segmented prepositive wing–main blade composite configuration is further studied.

This work is structured as follows: In Section 2, The horizontal axis wind turbine model, meshing method, and calculation method used in this paper are described. The mesh independence verification and the comparison between the calculated values and the experimental values are carried out, and the flow separation on the blade surface of the wind turbine under different wind speed conditions is analyzed. Then, in Section 3, the method of using a prepositive elliptical wing configuration to control the flow of the wind turbine blade in order to improve the aerodynamic performance of wind turbine is proposed, and this method is explored using an S809 airfoil. In Section 3.1, the flow control mechanism of the prepositive wing–main wing composite configuration is explained. In Section 3.2, the two-dimensional configuration is designed, including the shape, size, and position of the prepositive wing. In Section 3.3, the control effect of the prepositive wing–main wing composite configuration is shown, the flow control mechanism is analyzed, and the design space that can play an effective role in the wind turbine blade airfoil is determined. Based on Section 3, Section 4 extends the design of the composite configuration to three dimensions. Section 4.1 shows the design of the three-dimensional segmented prepositive elliptical wing–main blade configuration. Section 4.2 calculates five different composite configurations and compares them with the performance of the original wind turbine. Section 4.3 analyzes the reasons why the composite configuration improves the performance of the wind turbine from different perspectives, such as flow separation and surface pressure. Some useful conclusions are given in Section 5.

## 2. Numerical Simulation of Horizontal Axis Wind Turbine

The experimental design of this paper is divided into two parts according to the two-dimensional and three-dimensional situation. Firstly, the combined configuration of the wind turbine blade airfoil and the elliptical wing is designed, and the influence of the nine position schemes and sizes of the elliptical wing on the aerodynamic performance is studied in sequence. Secondly, based on the two-dimensional optimal scheme, five three-dimensional configurations are used to study the influence of the elliptical wing on the flow field characteristics of the composite configuration with different blade spans. In this way, the optimal configuration scheme of prepositive elliptical wing–main blade composite configuration is obtained, and their applicability in the real situation is evaluated.

### *2.1. Calculation Method and Mesh Division*

Since the torsion angles of wind turbine blades are large and airfoils are relatively thick, obvious flow separation occurs easily at a large deflection angle, thus affecting the efficiency of power generation. This study is based on the typical NREL Phase VI wind turbine with an S809 airfoil.

For the two-dimensional case, the unstructured polyhedral mesh was used for the calculation. The chord length of the S809 airfoil is c = 1 m, and the radius of the computational domain is 50 times the chord length of the airfoil. To make the numerical calculation more accurate, the model is stretched 1 m along the spanwise direction to generate a three-dimensional mesh, and the number of the mesh is approximately 1.1 million. Taking the configuration of setting a small ellipse at 5%c above the leading edge of the airfoil as an example, $L_1 = 0$, and $L_2 = 0.05$ m. The mesh and boundary conditions used in the calculation are shown in Figure 1.

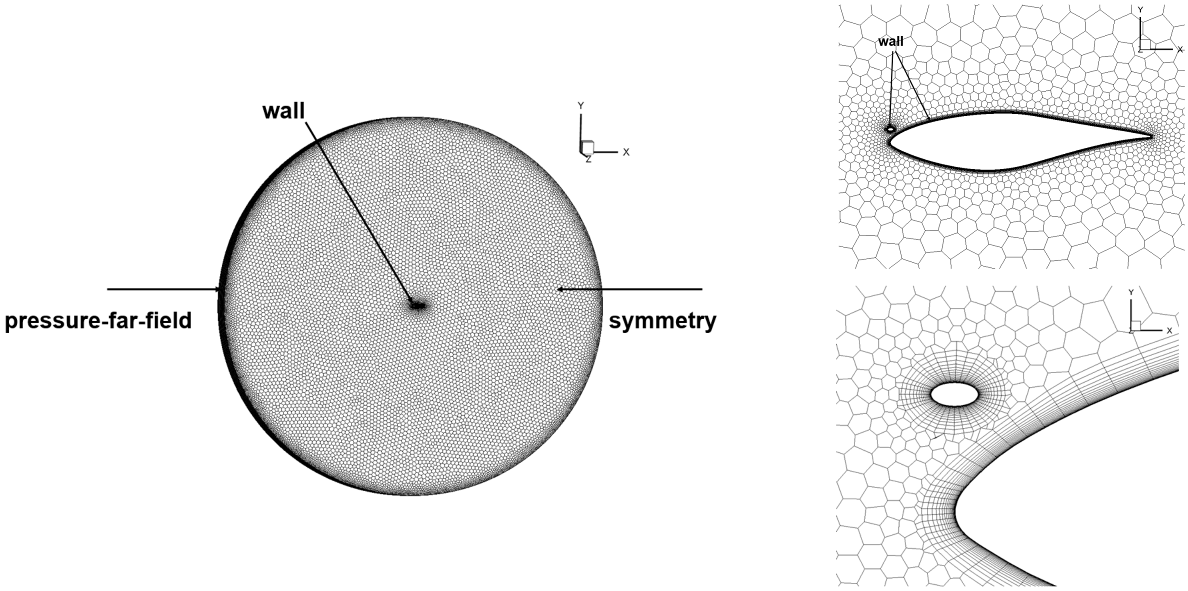


**Figure 1.** Computational mesh and boundary conditions.

For the three-dimensional case, since incoming wind speed is parallel to the rotor shaft, the model uses one blade to simplify the calculation, and a periodic boundary condition is adopted at the junction. The calculation domain is a semicylinder containing the blade with a radius of 50 m. The flow inlet and outlet are 50 m and 75 m from the blade center, respectively. The calculation uses an unstructured polyhedral mesh, and the boundary layer is set on the blade surface. The mesh division and boundary conditions are shown in Figure 2a, and the local surface mesh is shown in Figure 2b. The calculation conditions refer to the NREL aerodynamics experiment [25], as shown in Table 1.

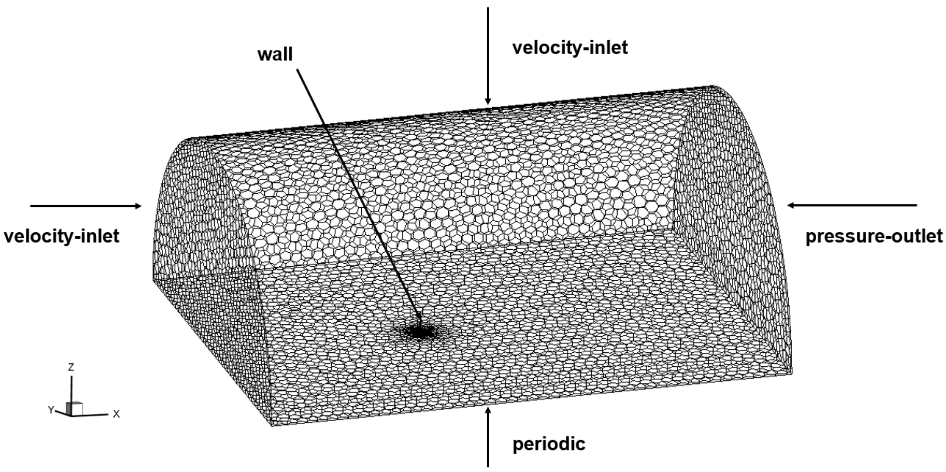


(**a**) Computational mesh and boundary conditions

**Figure 2.** *Cont*.

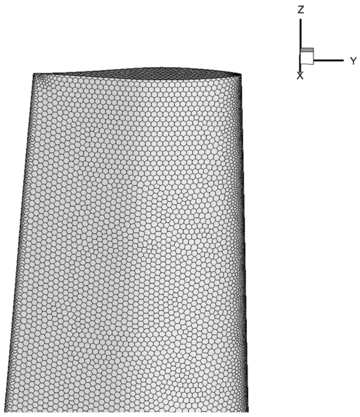


(**b**) Blade surface mesh

**Figure 2.** Computational mesh.

**Table 1.** Calculation conditions [25].

| Operational Condition | Rotating Speed [rpm] | Wind Speed [m/s] | Density [kg/m$^3$] | Viscosity $\times$ 10$^{-5}$ [kg/(ms)] |
|---|---|---|---|---|
| 1 | 71.9 | 7.0 | 1.246 | 1.769 |
| 2 | 72.1 | 10.0 | 1.246 | 1.769 |
| 3 | 72.1 | 13.0 | 1.227 | 1.781 |
| 4 | 72.1 | 15.1 | 1.224 | 1.784 |
| 5 | 72.0 | 20.1 | 1.221 | 1.786 |
| 6 | 72.1 | 25.1 | 1.220 | 1.785 |

In this paper, Fluent software is used for the numerical simulation, and the Navicr Stokes (N-S) equation solver, based on the finite volume method, is used. The second-order upwind scheme is used in the convection direction, the central difference is used in the diffusion term, and the coupled method is used in the pressure velocity coupling. The flow is compressible. The two-equation shear stress ($k-\omega$ SST) turbulence model [26] is used for the calculation, and the equation is expressed as:

$$\begin{gathered}\frac{\partial(\rho k)}{\partial t}+u_i\frac{\partial(\rho k)}{\partial x_i}=P_k-\beta_k\rho k\omega+\frac{\partial}{\partial x_i}\left[\left(\mu_l+\frac{\mu_t}{\sigma_k}\right)\frac{\partial k}{\partial x_i}\right]\\ \frac{\partial(\rho\omega)}{\partial t}+u_i\frac{\partial(\rho\omega)}{\partial x_i}=C_\omega P_\omega-\beta_\omega\rho\omega^2+\frac{\partial}{\partial x_i}\left[\left(\mu_l+\frac{\mu_t}{\sigma_\omega}\right)\frac{\partial\omega}{\partial x_i}\right]\\ +2\rho(1-F_1)\frac{1}{\sigma_{\omega2}}\frac{1}{\omega}\frac{\partial k}{\partial x_i}\frac{\partial\omega}{\partial x_i}\end{gathered} \tag{1}$$

The mesh independence is verified by the four mesh division schemes, which are shown in Table 2. Figure 3 shows that the torque numerical simulation results of Schemes 1 and 2 are quite different from the simulation results of Schemes 3 and 4. As the number of the mesh increases, the numerical simulation results of torque tend to be stable. The torque differences with Schemes 3 and 4 are less than 3% at each wind speed, and the maximum error is 2.67% at 13 m/s wind speed, which meets the requirements of grid independence. Considering the subsequent need to add a small elliptical wing at the leading edge of the blade, to better capture the details of the flow field around the blade and elliptical wing, Scheme 4 is used in the subsequent numerical simulation.

**Table 2.** Mesh division schemes.

| Scheme | y+ | Minimum Mesh Size (mm) | Maximum Mesh Size (mm) | Total Mesh Numbers (million) |
|---|---|---|---|---|
| 1 | 1 | 1 | 5000 | 1.21 |
| 2 | 1 | 0.5 | 3000 | 2.54 |
| 3 | 1 | 0.2 | 3000 | 5.02 |
| 4 | 1 | 0.1 | 3000 | 9.86 |

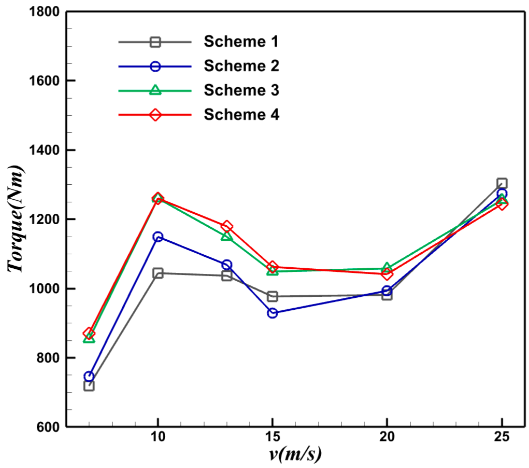


**Figure 3.** Mesh independence verification.

## 2.2. Case Verification

According to the experimental values, the Mach number is set to 0.042, and the Reynolds number is set to $1 \times 10^6$. First, the variation in the lift and drag coefficients of a single S809 airfoil with the angle of attack is simulated. The radius of the computational domain is 50 times the chord length of the airfoil. The comparison between the calculated and experimental values is shown in Figure 4. The lift and drag coefficients obtained by the experiment [25] are consistent with the simulation results in this paper, and the error is within the allowable range. In general, the computational mesh and numerical simulation method adopted are reliable.

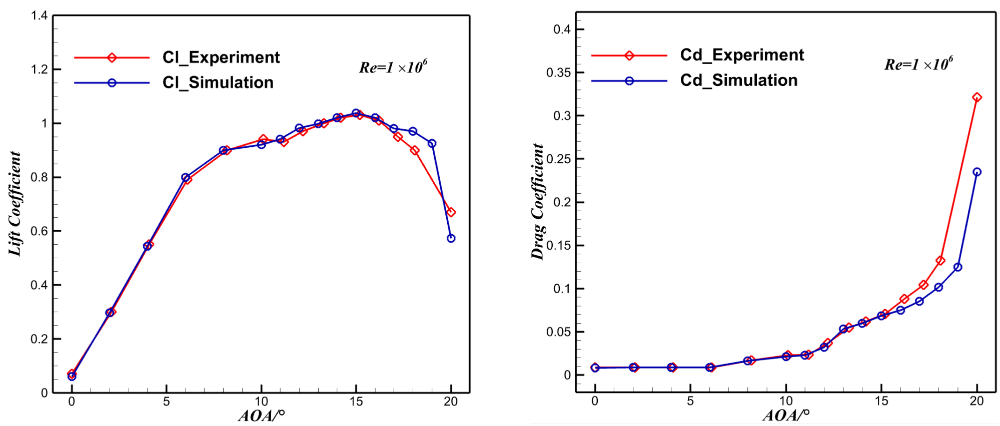


(**a**) Lift coefficient (**b**) Drag coefficient

**Figure 4.** Comparison of calculated and experimental [25] values.

Figure 5 shows the comparison between the simulated and experimental values of the wind turbine shaft torque. The simulation result curve is basically consistent with the curve of the law of torque variation with wind speed in the experiment, and the calculated value is in good agreement with the experimental value. The average error between the calculated shaft torque and the experimental value at six different wind speeds is 9.27% and the maximum error is 15.91% at 25 m/s wind speed, which is within the acceptable range, proving the effectiveness and accuracy of the numerical method.

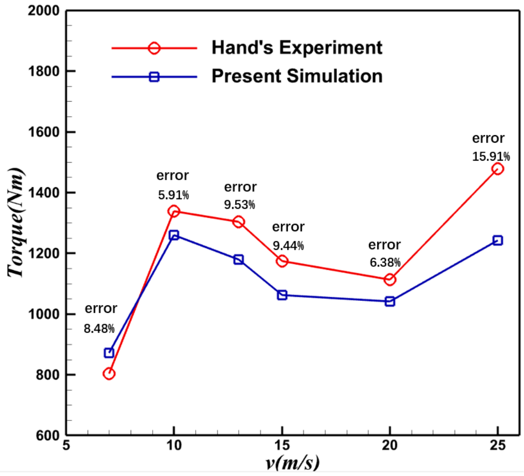


**Figure 5.** Comparison of calculated and experimental [25] values of wind turbine shaft torque.

Figure 6 shows the calculated limit streamline of the wind turbine blade suction side at the wind speed of 7~25 m/s. Owing to the three-dimensional rotation effect of the wind turbine blade, the Coriolis force, centrifugal force, and pressure difference in the wingspan direction act on the blade together. As the wind speed gradually increases, the range of the flow disorder region on the suction surface gradually increases. This separation trend gradually spreads from the root position to the tip area, and the flow separation point extends from the trailing edge area to the leading edge area. When the wind speed is 7 m/s, the flow field structure near the blade root area is relatively complex, and the flow around the hub is separated. When the wind speed is 10 m/s, the separation zone expands along the radial direction, and separation occurs at a position exceeding 90% of the suction surface, which affects the aerodynamic characteristics of the whole blade, and the blade stalls. If the wind speed increases above 15 m/s, the blade will enter the deep stall state, and the flow in the whole blade range will be separated. Flow separation seriously affects the aerodynamic power output of blade, resulting in power loss of the wind turbine. For a certain wind speed, stalling of the blade root is the most serious in the whole blade area, and stalling of the blade tip occurs only at high wind speeds. Additionally, wake structure after flow separation is very complex. Not only do vortices form in the separated wake and develop downstream, forming a spiral flow structure, but they also flow along the radial direction, forming a complex three-dimensional flow structure.

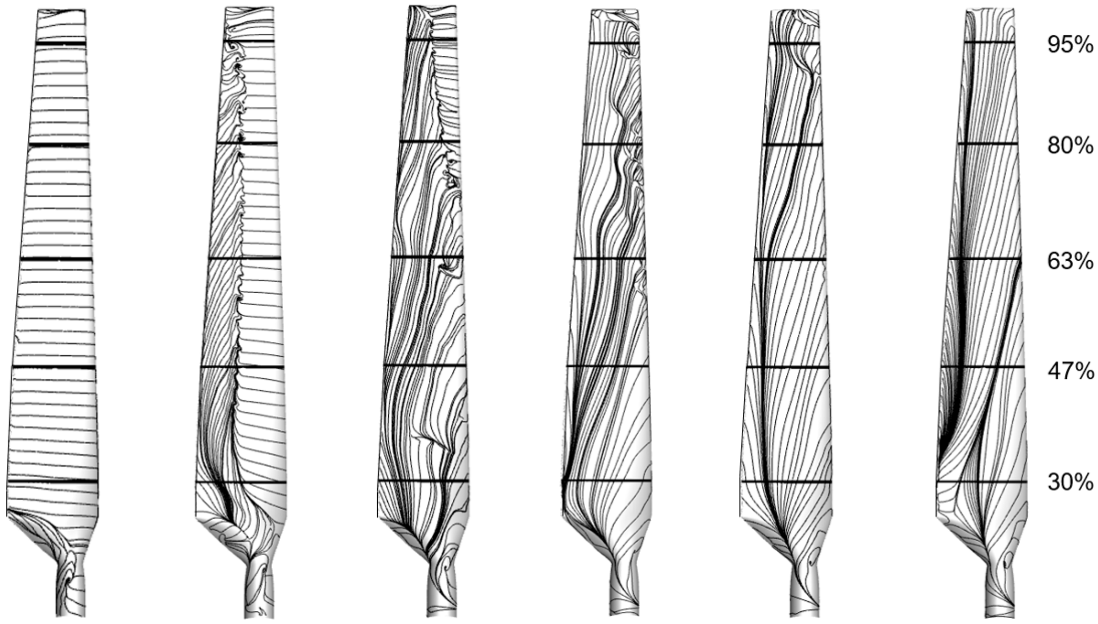


(**a**) 7 m/s (**b**) 10 m/s (**c**) 13 m/s (**d**) 15 m/s (**e**) 20 m/s (**f**) 25 m/s

**Figure 6.** Limiting streamlines on the blade suction surface.

## 3. Flow Control Method of Prepositive Elliptical Wing Configuration for Separated Flow

### *3.1. Flow Control Mechanism of Prepositive Elliptical Wing Configuration*

In this paper, the flow control mechanism of the prepositive elliptical wing configuration can be explained from three aspects, as shown in Figure 7. First, the elliptical wing placed around the leading edge of the airfoil or blade can be regarded as a special detached vortex generator. Similar to the conventional vortex generator, the prepositive elliptical wing can produce a high-energy wake vortex and mix with the downstream low-energy boundary layer flow; then, it can play a role in flow control. Second, the gap between the prepositive wings and the airfoil or blade has a similar effect to the leading-edge slat. It can significantly improve the aerodynamic characteristics by better resisting the boundary layer. Third, as a typical bluff body, the flow around the cylinder or elliptical cylinder has been studied extensively [27–29]. The unsteady shedding vortex is generated when the fluid flows through the elliptical wing, which is accelerated by the airflow on the suction surface into the separation airflow to increase the energy of the airflow and to suppress flow separation.

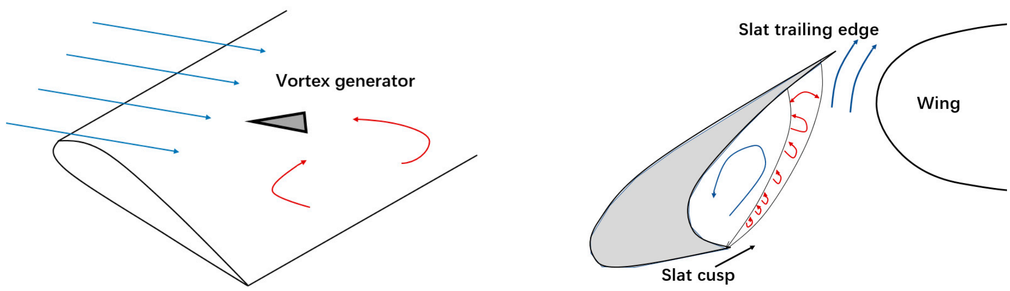


(**a**) Vortex generator (**b**) Leading edge slat

**Figure 7.** *Cont*.

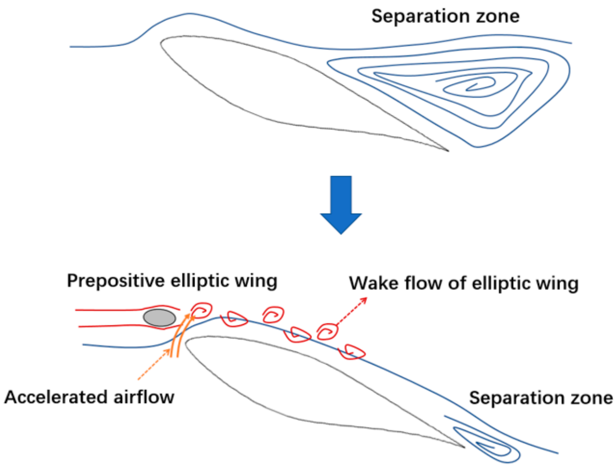


(**c**) Prepositive wing configuration

**Figure 7.** Flow control principle of prepositive wing configuration.

*3.2. Design of the Prepositive Wing–Main Wing Composite Flow Control Configuration Based on the S809 Airfoil*

According to blade element momentum theory, the wind turbine blade can be divided into several independent blade element infinitesimals along the spanwise direction. The force acting on each blade element is only determined by its airfoil lift–drag characteristics. By integrating the moment and force on blade element, the moment and force which act on the blade can be further derived. That is, the aerodynamic characteristics of the airfoil can determine the performance of the blade to a certain extent.

In this paper, a prepositive elliptical wing with a new configuration is proposed. An S809 airfoil is taken as the research object, and its chord length is c. A small elliptical wing with a long axis size of 2%c and a short axis size of 1%c is set near the leading edge. The horizontal distance between the center of elliptical wing and leading edge of the airfoil is $L_1$, and their vertical distance is $L_2$. Two groups of small circles with diameters of 2%c and 1%c are selected for comparison, and the positions are set to be the same as those of the elliptic wing. The influence of their sizes and positions on the flow control effect are studied. The calculation model and size are shown in Figure 8.

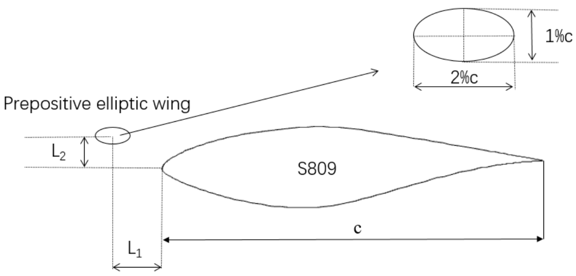


(**a**) Position relationship

**Figure 8.** *Cont.*

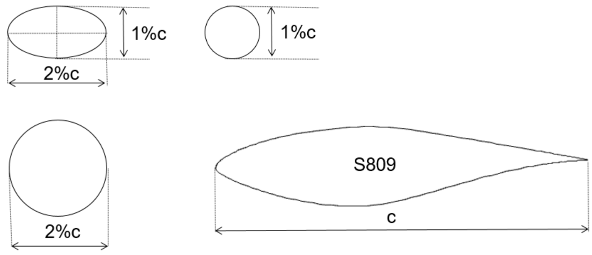


(**b**) Size relationship

**Figure 8.** Calculation model and size.

To further explore the flow control mechanism of this new configuration and clarify the influence of setting the position and size factors of the elliptical wing on the aerodynamic performance of an S809 airfoil, nine position schemes of the prepositive small elliptical or circular configuration are adopted to calculate, as shown in Table 3 and Figure 9.

**Table 3.** Position schemes of the prepositive wing configuration.

| **Original Airfoil** | S809 | **Scheme 5** | $L_1$ = 5%c, $L_2$ = 0 |
|---|---|---|---|
| **Scheme 1** | $L_1$ = 0, $L_2$ = 3%c | **Scheme 6** | $L_1$ = 7%c, $L_2$ = 0 |
| **Scheme 2** | $L_1$ = 0, $L_2$ = 5%c | **Scheme 7** | $L_1$ = 0, $L_2$ = −3%c |
| **Scheme 3** | $L_1$ = 0, $L_2$ = 7%c | **Scheme 8** | $L_1$ = 0, $L_2$ = −5%c |
| **Scheme 4** | $L_1$ = 3%c, $L_2$ = 0 | **Scheme 9** | $L_1$ = 0, $L_2$ = −7%c |

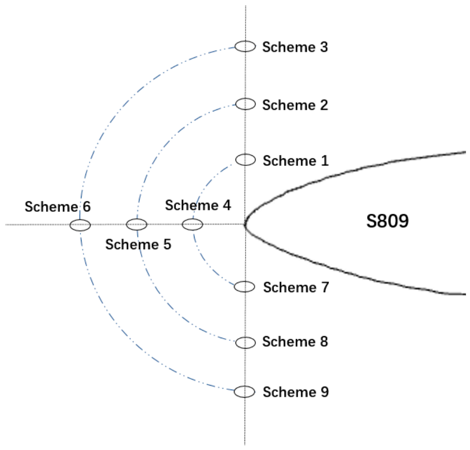


**Figure 9.** Schemes of prepositive wing configuration position.

*3.3. Evaluation of the Flow Control Effect of the Two-Dimensional Configuration*

The lift–drag ratios of the three configurations at different attack angles in nine position schemes are compared with those of the single S809 airfoil. In general, to increase lift–drag ratio of the airfoil and delay the stall attack angle, the most ideal control effect can be reached when the small component is set at a position 5%c to 7%c directly above the leading-edge point of S809 airfoil. The application range of the smaller component is larger, especially when the setting position is less than 5%c from the airfoil, and the size of the component must be reduced. When the small component is directly set in front of the S809 airfoil's leading-edge point, it should be at least 7%c from the leading-edge point, or the component which has a very small size must be set within 3%c near the leading-edge point. When small component is set directly below the S809 airfoil, leading-edge point, compared to the original airfoil, and the lift–drag ratio increases or approaches, in most cases. The control effect is highly dependent on the setting position, and the size change of the component within the acceptable range does not affect it. In addition, for a small angle of attack, these small components inevitably reduce the lift–drag ratio of the S809 airfoil.

To further clarify the flow control mechanism of the prepositive microparts on the airfoil, Figure 10 shows the velocity contours, pressure contours and streamlines of different position scheme configurations at 20° attack angle. By comparison, the position selection of Scheme 2 is optimal. When the ellipse and the circle with a diameter of 2%c are set, the flow control effect of these configurations is obvious, and the separation bubble near the original airfoil's trailing edge completely disappears. When Schemes 1 and 3 are adopted, setting the diameter of the 1%c circle can also move the separation point backward and make the separation bubble shrink. Except for Schemes 1–3, the other position schemes have no obvious inhibitory effect on the separation vortex generated by the airfoil. Comparing the velocity contours, the inhibiting effect of these prepositive wing configurations on flow separation is mainly that acceleration of the air flow through the upper surface of the airfoil increases the attachment energy of the air flow in the boundary layer of the upper surface, which delays the development of separation by better resisting the boundary layer separation. When the component is too large for the set position, it will hinder the original flow on the wing surface and deteriorate the S809 airfoil aerodynamic performance, such as in Scheme 1.

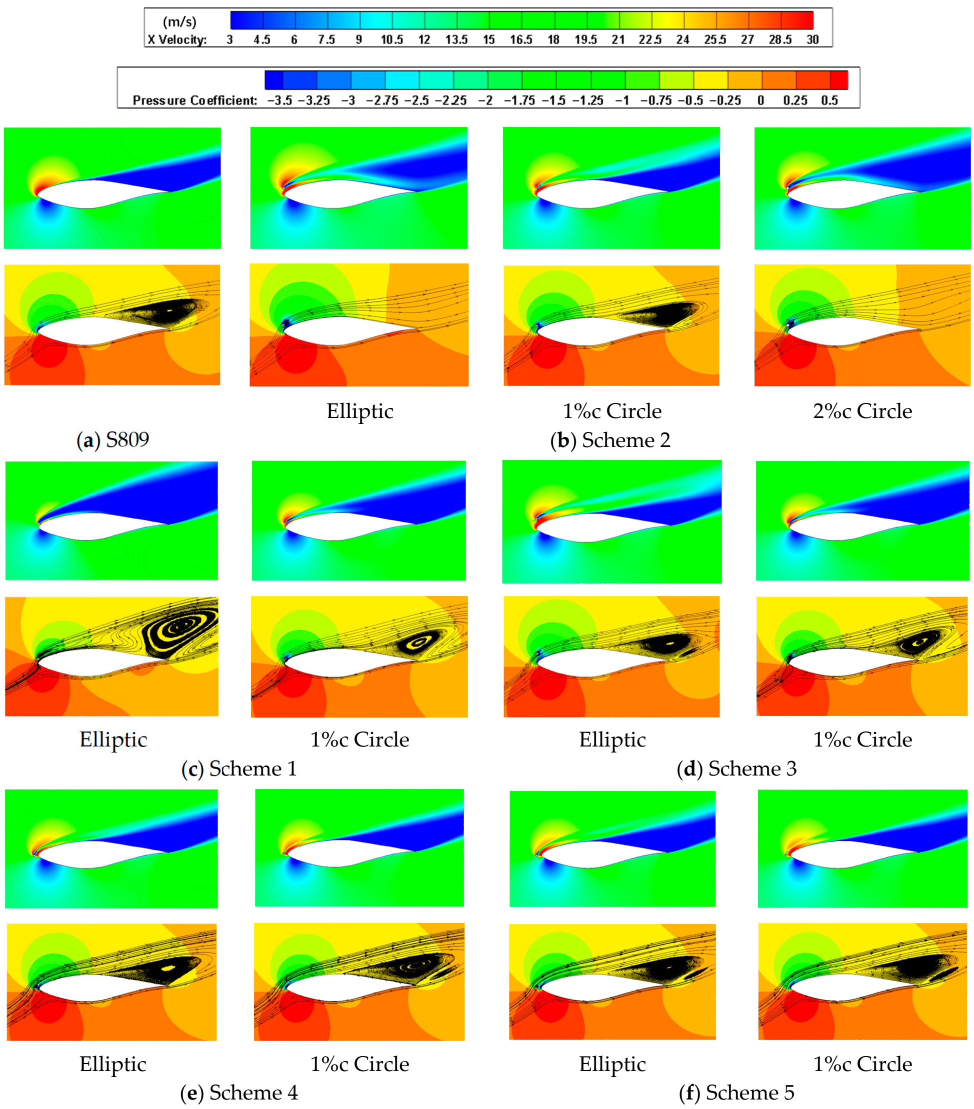


**Figure 10.** *Cont.*

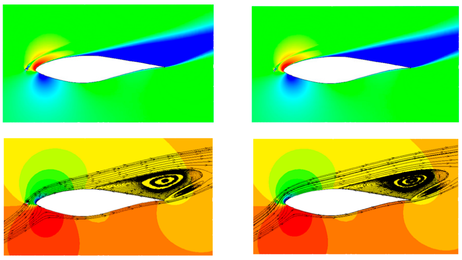

Elliptic 1%c Circle

(**g**) Scheme 6

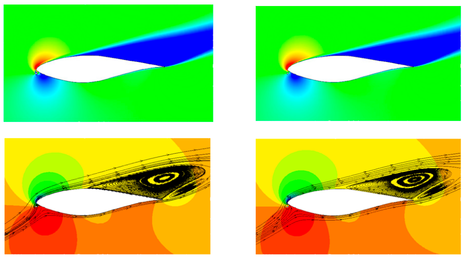

Elliptic 1%c Circle

(**h**) Scheme 7

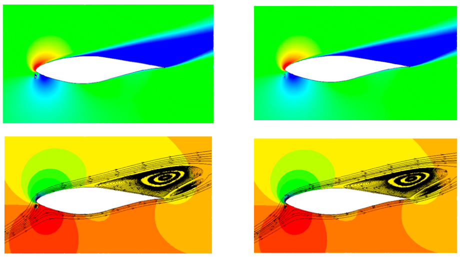

Elliptic 1%c Circle

(**i**) Scheme 8

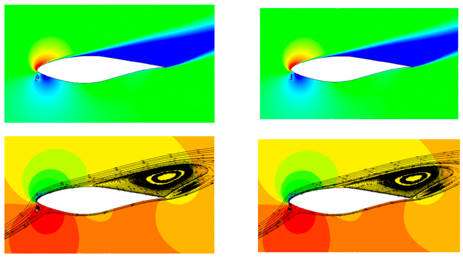

Elliptic 1%c Circle

(**j**) Scheme 9

**Figure 10.** Velocity contours, pressure contours, and streamlines of different configuration schemes at 20° attack angle.

Figure 11 shows the comparison of the pressure coefficients of several different position configurations with the S809 airfoil at 20° attack angle. In general, compared with that of the original S809 airfoil, the pressure coefficient of the effective prepositive wing configuration's suction surface is significantly reduced, while the pressure surface's pressure coefficient is slightly increased, which makes the airfoil surface pressure difference increase and then increase airfoil lift. In contrast, the ineffective prepositive wing configuration increases the suction surface pressure coefficient of the original airfoil and decreases the pressure coefficient of the pressure surface, as shown in Figure 11c,f. The same is true in that the prepositive wing has a more pronounced effect on the pressure coefficient of the airfoil suction surface.

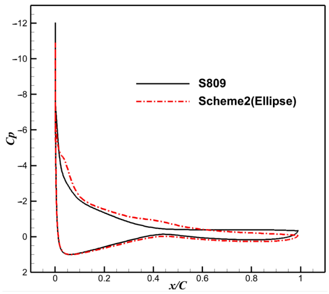


(**a**) Scheme 2

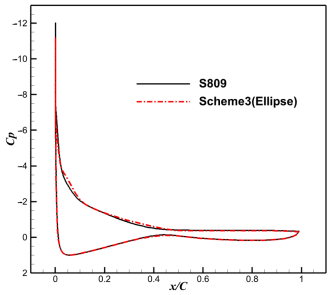


(**b**) Scheme 3

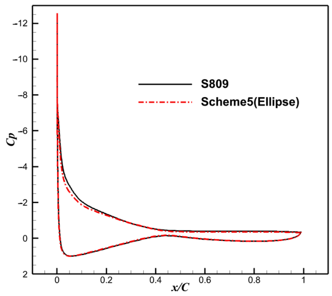


(**c**) Scheme 5

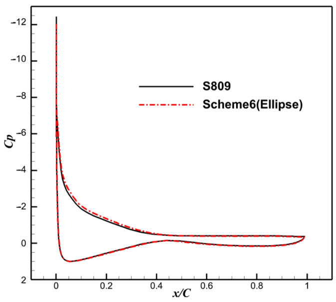


(**d**) Scheme 6

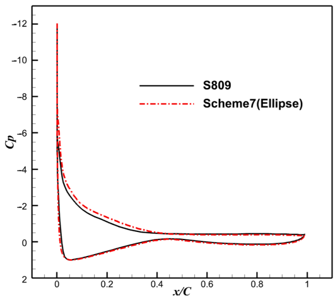


(**e**) Scheme 7

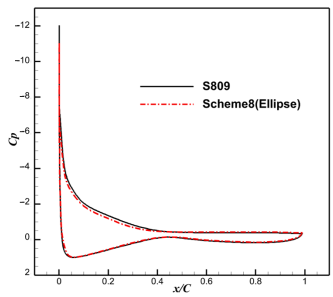


(**f**) Scheme 8

**Figure 11.** Pressure coefficient curves of different configurations at 20° angle of attack.

## 4. Flow Control Scheme Design Based on Segmented Prepositive Elliptical Wing–Main Blade Composite Configuration

### *4.1. Design of Segmented Prepositive Elliptical Wing–Main Blade Composite Configuration*

For purpose of studying the application effect of the prepositive elliptic wing as a passive flow control component on the blade, and to further clarify the influence of the setting method on the wind turbine performance, according to the calculation results of setting a prepositive elliptical wing with different sizes and positions in front of the S809 airfoil in Section 3.3, the position of Scheme 2 ($L_1$ = 0, $L_2$ = 5%c) should be adopted. The segmented front ellipse is positioned just above the airfoil leading-edge point with the long axis size of 2%c and short axis size of 1%c. Due to the blade section, the airfoil has different chord lengths; the long axis size of the elliptical wing should not be greater than 2% of the minimum section airfoil's chord length. The horizontal distance $L_1$ from the center to the leading edge of the blade section of the airfoil is 0, and the vertical distance $L_2$ is within 5%c~7%c.

The elliptical wing is arranged at the S809 airfoil from the cross section of the wind turbine blade, that is, 25% of the entire blade. A segment is arranged every 15% length in the direction of wing tip, and the elliptical wing blades are divided into 5 segments. As shown in Figure 12a, the elliptical wing's size is calculated from the minimum section chord near the wing tip in each segment to ensure that the elliptical wing's overall size is sufficiently small. The position is calculated from the maximum section chord near the blade root in each segment to ensure that the horizontal and vertical distance between the center of elliptical wing and the leading-edge point of the blade section airfoil meet the requirements. The elliptical wing's twist angle is the same as the blade's, on this basis, as configuration 1. Then a new configuration is formed by successively reducing a segment of the elliptical wing from the blade root to tip, which is reduced for four times in total, and five composite configurations of the prepositive elliptical wing–main blade are obtained. Some studies [23,24] have shown that the conventional vortex generator, based on a two-dimensional airfoil design, has difficulty in achieving the desired effect when applied to a three-dimensional blade because the vortex generator will be easily submerged in the trailing edge separation bubble at the root of the blade or lead to an early sudden stall of the blade. Therefore, when extending the two-dimensional results to three-dimensional, it is necessary to compare the performance of different three-dimensional segmented prepositive elliptical wing–main blade configurations. Figure 12b–d show the composition of configuration 1, configuration 2, and configuration 5, respectively.

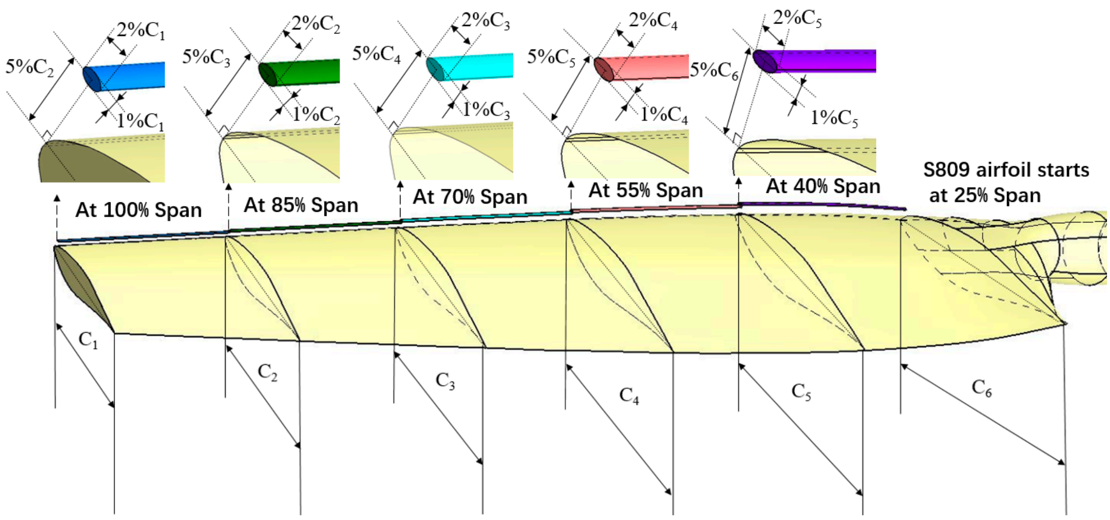


(**a**) Size and position diagram

**Figure 12.** *Cont.*

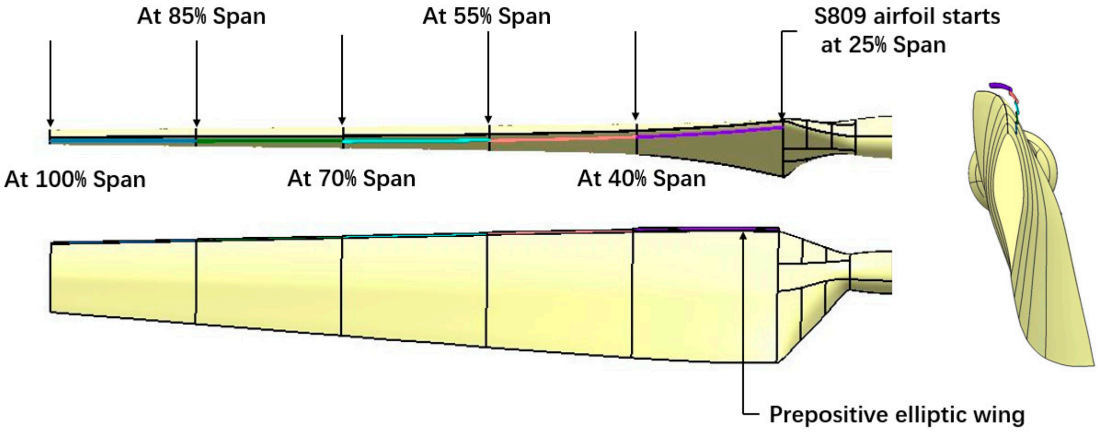


(**b**) Composite configuration 1

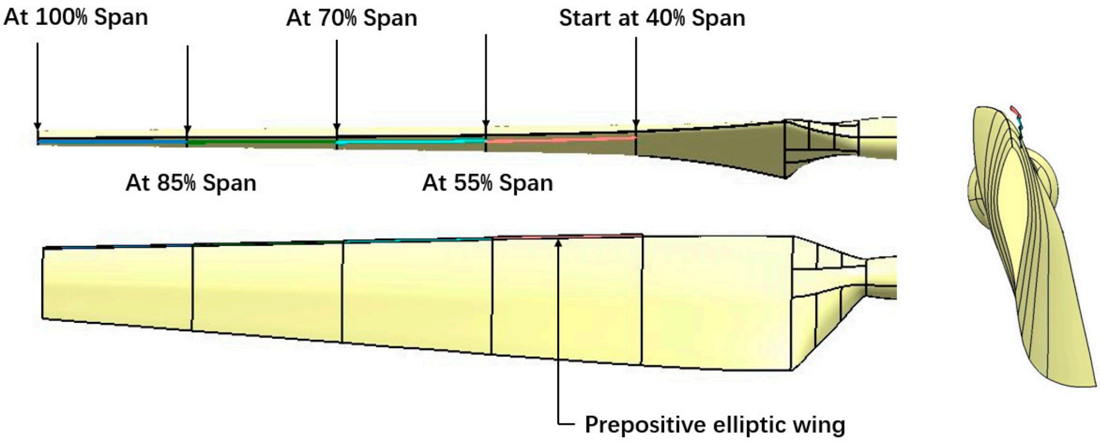


(**c**) Composite configuration 2

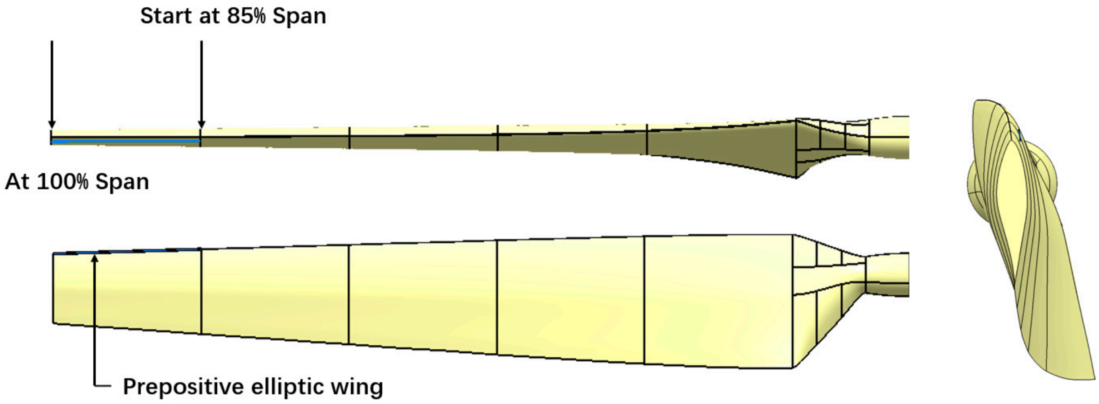


(**d**) Composite configuration 5

**Figure 12.** Segmented prepositive elliptical wing–main blade composite configuration.

### 4.2. Simulation Verification of Composite Configurations' Flow Control Effect

The five composite configurations are calculated using the calculation conditions in Table 1, and they use the same mesh conditions as Scheme 4 in Table 2. The results are shown in Figure 13. At 7 m/s wind speed, all five configurations have a negative impact on the blades, reducing the torque by approximately 5% on average. At 10 m/s wind speed, except for configuration 5, the other four configurations all improve the torque of the original blade. When the wind speed is greater than 13 m/s and less than 20 m/s, all five configurations can increase the torque. Among them, configuration 1 can increase the torque by more than 30%, which is the best effect, while the torque growth rate of the other configurations decreases successively. Configuration 5 has the worst control effect, as it only increases the torque by approximately 6% when the wind speed is 15 m/s. However, when the wind speed is greater than 20 m/s, configurations 4 and 5 have the least influence on the original blade, and the blade torque is almost unchanged, while configurations 1, 2, and 3 slightly reduce the blade torque by 2% at high wind speeds. This shows that the prepositive elliptical wing configuration can be applied to a three-dimensional blade, and the effect of the full segment setting is the best. When the elliptical wing is set above 70% of the blade span, the torque at a high wind speed is no longer affected, as in configurations 4 and 5. In addition, consistent with the two-dimensional calculation results, the prepositive elliptical wing configuration reduces the lift–drag ratio of the airfoil at a low attack angle, and segmented prepositive elliptical wing–main blade composite configurations also reduce the blade torque at a low wind speed of 7 m/s.

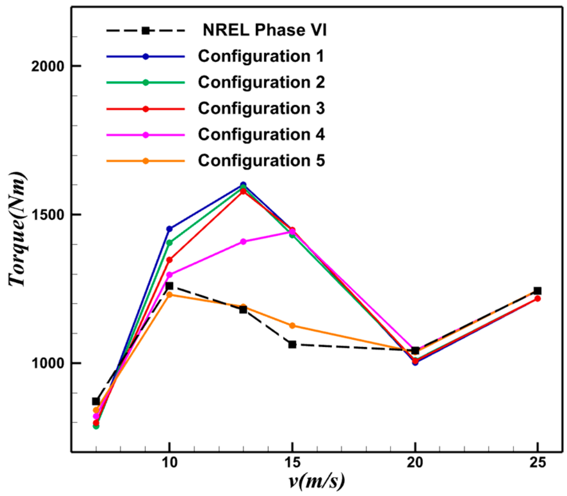


**Figure 13.** Torque of original blade and five composite configurations.

### *4.3. Analysis of Flow Field Improvement Mechanism of a Three-Dimensional Blade with a Composite Configuration*

By comparing the limiting streamline of the wind turbine blade suction surface, the influence of the segmented prepositive elliptical wing–main blade composite configuration with different heights on flow separation of blade is studied. Since the calculated aerodynamic performance parameters of the five configurations are basically reduced with the number of configurations, only configurations 1, 3, and 5 are selected for analysis. Figure 14 shows the comparison of limiting streamlines on the suction surface of the original blade and three composite configurations. At 7 m/s wind speed, configuration 1 hardly changes the flow state of the attached flow on the original blade, and limiting streamlines at the blade root trailing edge under 47% of the blade span position of configurations 3 and 5 squeeze slightly upward. At wind speeds of 10~15 m/s, configurations 1 and 3 have obvious effects on flow control. Part of the flow separation on the suction surface of the original blade is suppressed due to the attached flow from the blade tip. Part of the flow separation on the suction surface of original blade is suppressed from tip to the attached flow. The separation point is close to the blade root, and spanwise separation flow is reduced, which improves the torque of the blade. Configuration 5 also has an obvious inhibitory effect on flow separation at wind speeds of 13~15 m/s, and it increases the range of attached flow starting from the blade tip. At wind speeds of 20~25 m/s, flow separation covers the suction surface of configurations 1, 3, and 5, and the blade enters the deep stall state. At this time, the configuration cannot exert the flow control effect.

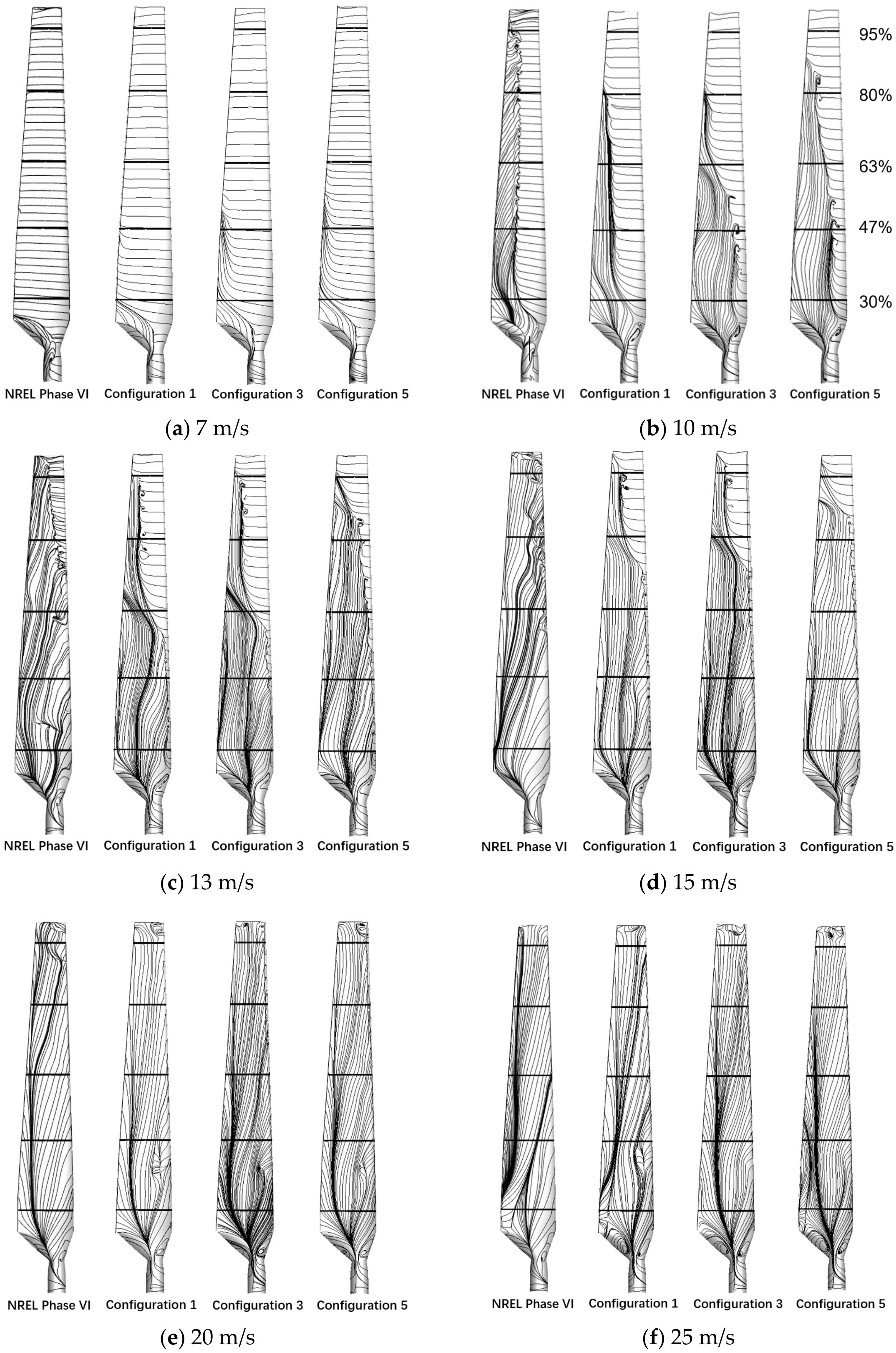


**Figure 14.** Limiting streamlines on blade suction surface.

To demonstrate the inhibitory effect of the new composite configuration on the flow separation of the blade, taking 13 m/s wind speed as an example, the streamlines at 95%, 80%, 63%, and 47% of the blade span positions of the original blade and configurations

1, 3, and 5 are shown in Figure 15. At 95% of the blade span section, configurations 1, 3, and 5 all have flow control effects, and the small separation vortex at the trailing edge of the original blade is suppressed to laminar flow. At 80% and 63% in the section location, the original model blade exhibits serious flow separation, and a large separation vortex is generated on the blade surface. At this time, configurations 1 and 3 can still play a role, and the inhibition effect on flow separation is significant. Thus, the separation vortex disappears completely. However, configuration 5 does not exert a control effect, and the vortex structure on the surface of blade is similar to that of the original blade. At 47% of the blade span, separation on the blade is intensified, and none of the three configurations are effective. Since configuration 5 only inhibits flow separation at the 95% blade span position, the torque of configuration 5 is only 0.85% higher than the original blade, while torques of configuration 1 and configuration 3 are increased by 35.5% and 33.8%, respectively. Moreover, the segmented prepositive elliptical wing–main blade configuration does not cause the blade to suddenly stall early and does not further expand the separation vortex, even if the flow control effect is not achieved.

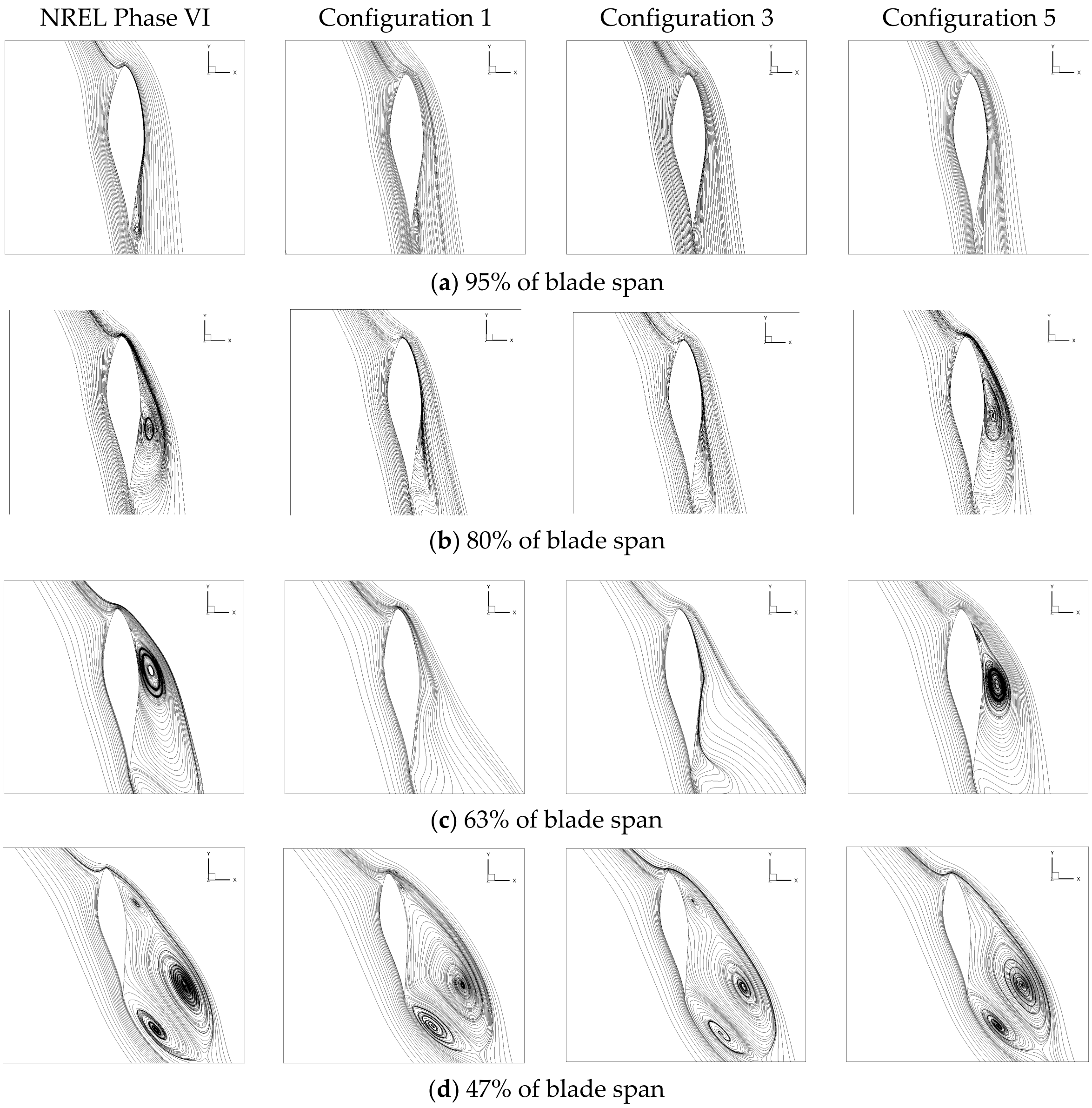


**Figure 15.** Streamline distribution of different cross sections of blade span at 13 m/s wind speed.

Figures 16 and 17 show the pressure contours on the suction and pressure surface of original blade and configurations 1, 3, and 5. The comparison shows that the three configurations have the same pressure distribution characteristics as the original blade. At 7 m/s wind speed, the pressure at the trailing edge of the suction surface of configurations 1 and 3 increases slightly. Meanwhile, the pressure surface is basically unchanged, the pressure difference on the blade surface decreases, and the torque also decreases. The pressure distribution contours of configuration 5 are very similar to the original blade, and the torque is only reduced by 3.4%. At wind speeds of 10~15 m/s, the pressure at the blade tip leading edge of the suction surface of configurations 1 and 3 obviously decreases, while the pressure at trailing edge of pressure surface increases. It increases the torque of the blade by increasing the pressure difference on the blade surface, therefore increasing the output power of the wind turbine. For configuration 5, pressure on the tip of the suction surface decreases, and pressure on the pressure surface increases only at wind speeds of 13 m/s and 15 m/s. Furthermore, at wind speeds of 20~25 m/s, the pressure distribution on blade suction surface is relatively complex, and the pressure of the three configurations on the pressure surface are almost the same as those of the original blade.

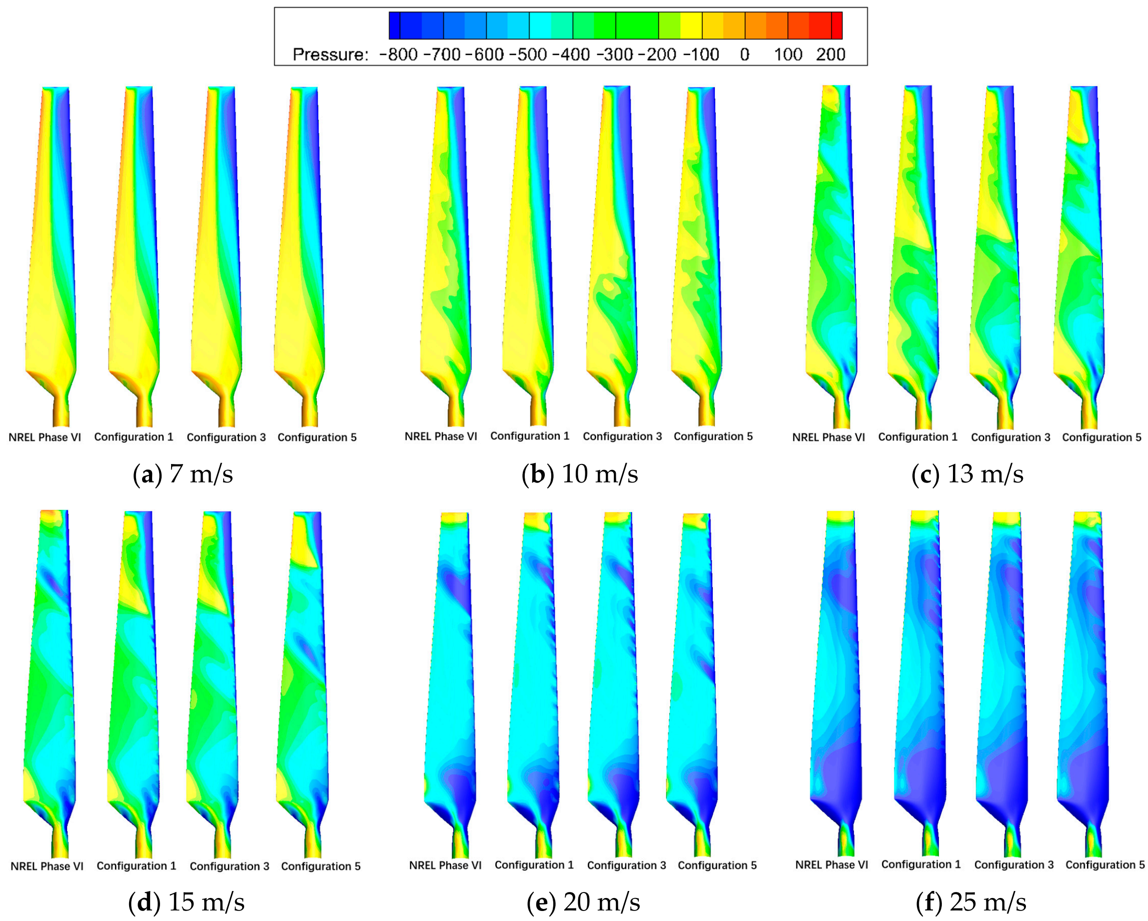


**Figure 16.** Pressure distribution of blade suction surface.

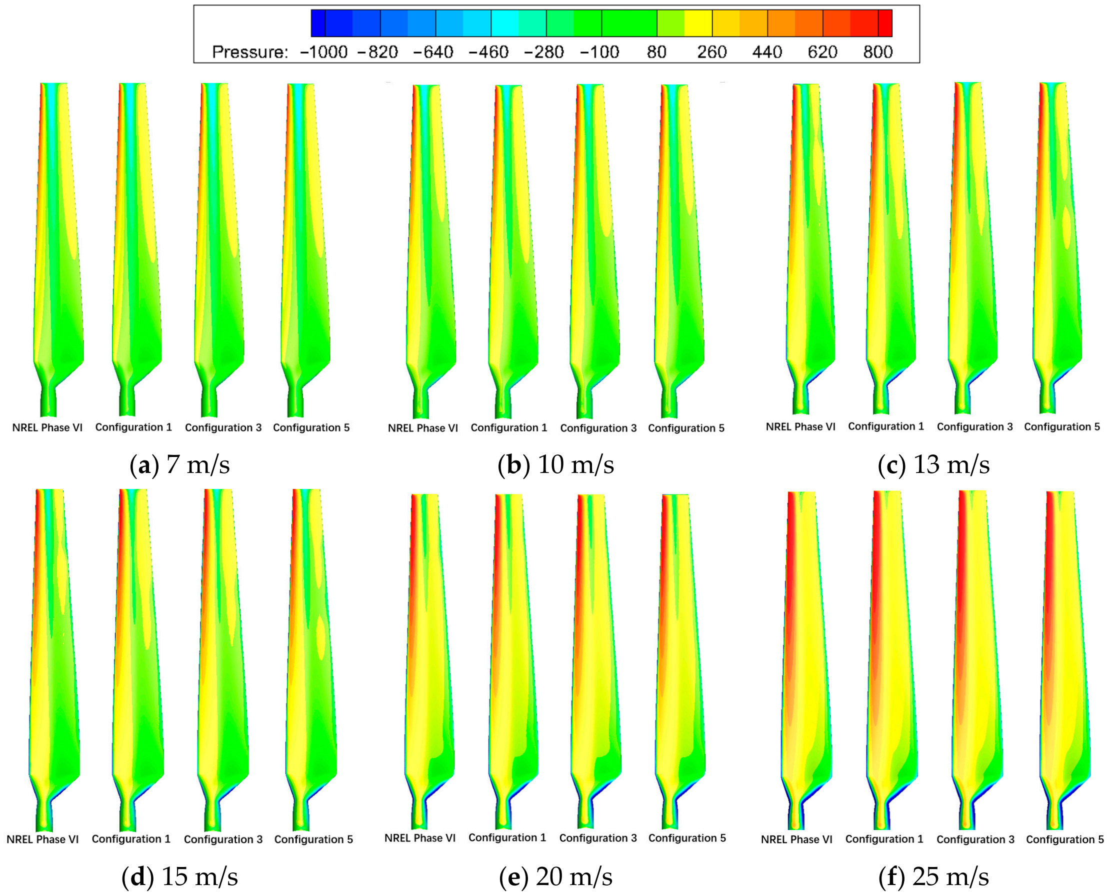


**Figure 17.** Pressure distribution of blade pressure surface.

Figure 18 shows the pressure coefficients of the original blade and three configurations with five sections at the wind speed of 20 m/s. Compared with the original blade, configurations 1, 3, and 5 mainly reduce the pressure difference at 80% of the blade span position. The pressure difference in configuration 5 at the 80% blade span section is greater than that of the original blade. According to the comparison of pressure difference, the aerodynamic performance of configurations 1 and 3 is slightly worse than that of the original blade at high wind speed, while configuration 5 is similar to the original blade. This result is the same as the calculation result of the torque. This also indicates that the segmented prepositive elliptical wing–main blade configuration can affect the performance of the wind turbine by changing the pressure distribution on blade surface.

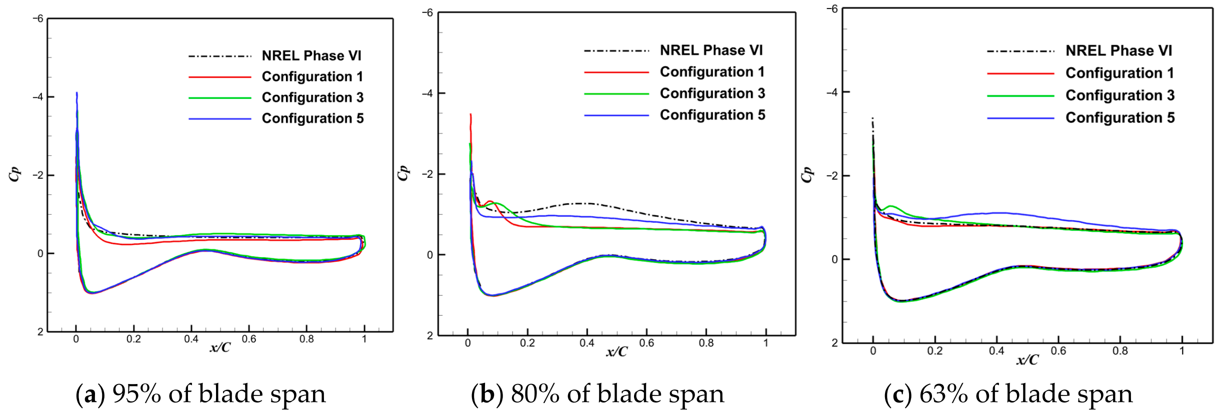


**Figure 18.** *Cont*.

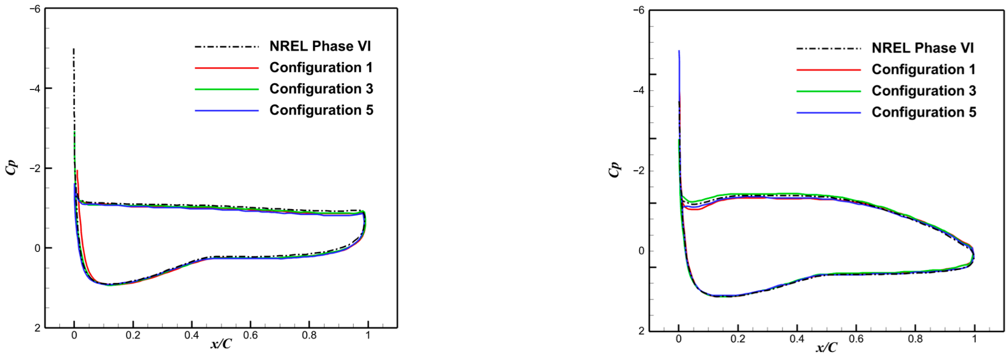


(**d**) 47% of blade span (**e**) 30% of blade span

**Figure 18.** Pressure coefficient of airfoils with different spanwise sections at 20 m/s wind speed.

## 5. Conclusions

A passive flow control method is innovatively proposed for a segmented prepositive elliptical wing–main blade composite configuration applied to a horizontal axis wind turbine in this paper. The flow separation is suppressed by setting the segmented small elliptical wing near the leading edge of the blade, thereby improving the wind turbine performance. The main conclusions are as follows:

1. Properly setting the small elliptical wing in front of the S809 airfoil can effectively delay the stall attack angle and increase the lift–drag ratio of airfoil. The most ideal control effect can be achieved when the elliptical wing is set 5%c–7%c above the leading-edge point, and a smaller component has a larger application range.
2. The prepositive elliptical wing configuration can be applied to a three-dimensional rotating blade through two-dimensional design. It does not suffer from the problem where it is submerged in the separation bubble and causes the blade to stall suddenly in the early stage when the conventional vortex generator is set at the downstream blade root. The performance of the wind turbine is the best when the prepositive elliptical wing is a full segment set.
3. At wind speeds of 10~20 m/s, the composite configuration can achieve a good flow control effect and increase the blade torque by approximately 35% at most. When the wind speed is greater than 20 m/s, the blade enters the deep stall state, and the composite configuration cannot suppress separation. The elliptical wing set in the whole section reduces the torque of the blade by 2%, while the elliptical wing set above 70% of the blade span has no effect on the torque of the original blade.
4. Through the analysis and comparison of flow field characteristics of the composite configurations and the original blade, the segmented prepositive elliptical wing–main blade configurations mainly improve the performance of the wind turbine by inhibiting flow separation on the blade and increasing the pressure difference between the suction and pressure surface. The most obvious change occurs at the leading edge of blade tip.
5. In real application situations, the optimal configuration of the proposed combination configuration is to add a detachable elliptical wing, which is parallel to the leading edge of the blade, at the position about 6%c from the leading edge of the blade, and the chord length of the elliptical wing refers to 1% of the blade tip chord length. This configuration can greatly improve the aerodynamic performance at medium wind speeds of 10~20 m/s, which is commonly used in wind turbines. In other small and large wind speeds, the elliptical wing can be removed, and the turbine only retains the original blade.

**Author Contributions:** Conceptualization, B.M.; methodology, X.B.; data curation, X.B.; resources, H.Z.; writing—original draft, X.B.; writing—review and editing, B.M. and H.Z.; supervision, H.Z.; project administration, H.Z. All authors have read and agreed to the published version of the manuscript.

**Funding:** This research was funded by the National Natural Science Foundation of China, Grant No. 12202363, the Fundamental Research Funds for the Central Universities, Grant No. G2020KY05115 and the support of Natural Science Basic Research Program of Shaanxi, Program No. 2021JQ-084.

**Conflicts of Interest:** The authors declare no conflict of interest.

## References

1. Kamari, D.; Tadjfar, M.; Madadi, A. Optimization of sd7003 airfoil performance using tbl and cbl at low reynolds numbers. *Aerosp. Sci. Technol.* **2018**, *79*, 199–211. [CrossRef]
2. Rodriguez, I.; Lehmkuhl, O.; Borrell, R. Effects of the actuation on the boundary layer of an airfoil at reynolds number = 60000. *Flow Turbul. Combust. Springer Neth.* **2020**, *105*, 607–626. [CrossRef]
3. Itsariyapinyo, P.; Sharma, R.N. Large eddy simulation of a naca0015 circulation control airfoil using synthetic jets. *Aerosp. Sci. Technol.* **2018**, *82–83*, 545–556. [CrossRef]
4. Zhu, H.; Hao, W.; Li, C. Simulation on flow control strategy of synthetic jet in a vertical axis wind turbine. *Aerosp. Sci. Technol.* **2018**, *77*, 439–448. [CrossRef]
5. Zong, H.; Van Pelt, T.; Kotsonis, M. Airfoil flow separation control with plasma synthetic jets at moderate reynolds number. *Exp. Fluids* **2018**, *59*, 1–19. [CrossRef]
6. Liu, Z.; Luo, Z.; Liu, Q. Modulation of driving signals in flow control over an airfoil with synthetic jet. *Chin. J. Aeronaut.* **2020**, *33*, 3138–3148. [CrossRef]
7. Nobari, M.R.H.; Mirzaee, E.; Nosratollahi, M. Improvement of wind turbine performance using a novel tip plate structure. *Energy Convers. Manag.* **2016**, *123*, 592–609. [CrossRef]
8. Khaled, M.; Ibrahim, M.M.; Hamed, H.E.A.; AbdelGwad, A.F. Investigation of a small Horizontal-Axis wind turbine performance with and without winglet. *Energy* **2019**, *187*, 115921. [CrossRef]
9. Mühle, F.; Bartl, J.; Hansen, T.; Adaramola, M.S.; Sætran, L. An experiments study on the effects of winglets on the tip vortex interaction in the near wake of a model wind turbine. *Wind. Energy* **2020**, *23*, 1286–1300. [CrossRef]
10. Mourad, M.G.; Shahin, I.; Ayad, S.S.; Abdellatif, O.E.; Mekhail, T.A. Effect of winglet geometry on horizontal axis wind turbine performance. *Eng. Rep.* **2020**, *2*, e12101. [CrossRef]
11. Wang, H.; Jiang, X.; Chao, Y. Effects of leading-edge slat on flow separation and aerodynamic performance of wind turbine. *Energy* **2019**, *182*, 988–998. [CrossRef]
12. Abate, G.; Mavris, D.N. Performance analysis of different positions of leading-edge tubercles on a wind turbine blade. In Proceedings of the 2018 Wind Energy Symposium, Kissimmee, FL, USA, 8–12 January 2018; pp. 1–11.
13. Abate, G.; Mavris, D.N.; Sankar, L.N. Performance effects of leading-edge tubercles on the NREL phase VI wind turbine blade. *J. Energy Resour. Technol.* **2019**, *141*, 051206.1–051206.9. [CrossRef]
14. Alber, J.; Soto-Valle, R.; Manolesos, M.; Bartholomay, S.; Nayeri, C.N.; Schönlau, M.; Menzel, C.; Paschereit, C.O.; Twele, J.; Fortmann, J. Aerodynamic effects of Gurney flaps on the rotor blades of a research wind turbine. *Wind. Energy Sci.* **2020**, *5*, 1645–1662. [CrossRef]
15. Yang, J.; Yang, H.; Zhu, W.; Li, I. Experimental Study on Aerodynamic Characteristics of a Gurney Flap on a Wind Turbine Airfoil under High Turbulent Flow Condition. *Appl. Sci.* **2020**, *10*, 7258. [CrossRef]
16. Zhu, H.; Hao, W.; Li, C.; Luo, S.; Liu, Q.; Gao, C. Effect of geometric parameters of Gurney flap on performance enhancement of straight-bladed vertical axis wind turbine. *Renew. Energy* **2021**, *165*, 464–480. [CrossRef]
17. Wang, H.P.; Zhang, B.; Qiu, Q.G.; Xu, X. Flow control on the NREL S809 wind turbine airfoil using vortex generators. *Energy* **2016**, *118*, 1210–1221. [CrossRef]
18. Troldborg, N.; Zahle, F.; Sorensen, N.N. Simulations of Wind Turbine Rotor with Vortex Generators. In *Science of Making Torque from Wind*, 2nd ed.; TORQUE 2016; Institute of Physics Publishing: Munich, Germany, 2016. [CrossRef]
19. Suarez, J.M.; Flaszynski, P.; Doerffer, P. Application of rod vortex generators for flow separation reduction on wind turbine rotor. *Wind. Energy* **2018**, *21*, 1202–1215. [CrossRef]
20. Mueller-Vahl, H.; Pechlivanoglou, G.; Nayeri, C.N.; Paschereit, C.O. Vortex generators for wind turbine blades: A combined wind tunnel and wind turbine parametric study. *New York Amer. Soc. Mech. Eng. Proc. ASME Turbo Expo.* **2012**, *6*, 899–914.
21. Baldacchino, D.; Ferreira, C.; De Tavernier, D.; Timmer, W.A.; van Bussel, G.J.W. Experimental parameter study for passive vortex generators on a 30% thick airfoil. *Wind. Energy* **2018**, *21*, 745–765. [CrossRef]
22. Lee, H.M.; Kwon, O.J. Numerical simulation of horizontal axis wind turbines with vortex generators. *Int. J. Aeronaut. Space Sci.* **2019**, *20*, 325–334. [CrossRef]
23. Dadamoussa, A.; Boualem, K.; Yahiaoui, T.; Imine, O. Numerical investigation of flow on a Darrieus vertical axis wind turbine blade with vortex generators. *Int. J. Fluid Mech. Res.* **2020**, *47*, 43–58. [CrossRef]

24. Zhu, C.; Chen, J.; Qiu, Y.; Wang, T. Numerical investigation into rotational augmentation with passive vortex generators on the NREL Phase VI blade. *Energy* **2021**, *1*, 120089. [CrossRef]
25. Hand, M.M.; Simms, D.A.; Fingersh, L.J.; Jager, D.W.; Cotrell, J.R.; Schreck, S.; Larwood, S.M. *Unsteady Aerodynamics Experiment Phase VI: Wind Tunnel Test Configurations and Available Data Campaigns. NREL/TP-500-29955*; U.S. Department of Energy Office of Scientific and Technical Information: Oak Ridge, TN, USA, 2001.
26. Patel, V.C.; Rodi, W.; Scheuerer, G. Turbulence models for near-wall and low Reynolds number flows: A Review. *AIAA J.* **1985**, *23*, 1308–1319. [CrossRef]
27. Chang-Yue, L.U. Large-Eddy and Detached-Eddy Simulations of the separated flow around a circular cylinde. *J. Hydrodyn. Ser. B* **2007**, *19*, 559–563. [CrossRef]
28. Lin, Y.J.; Miau, J.J.; Tu, J.K.; Tsai, H.W. Nonstationary, Three-Dimensional Aspects of Flow Around Circular Cylinder at Critical Reynolds Numbers. *AIAA J.* **2011**, *49*, 1857–1870. [CrossRef]
29. Mi, B.G.; Bai, X. New flow control techniques with prepositioned stationary or vibrating elliptical wing at low speed and high angle of attack. *J. Aerosp. Eng.* **2022**, *35*, 04022064. [CrossRef]